Diverse Image Priors for Black-box Data-free Knowledge Distillation

Anonymous authors
Paper under double-blind review

Abstract

Knowledge distillation (KD) is a well-known technique for effectively transferring knowledge from an expert network (teacher) to a smaller network (student) with little sacrifice in performance. However, most KD methods require extensive access to the teacher or even its original training set, which are unachievable due to intellectual property or security concerns. These challenges have inspired *black-box data-free KD*, in which only the teacher's top-1 predictions and no real data are available. While recent approaches tend to synthetic data, they largely overlook data diversity, which is crucial for effective knowledge transfer. We propose Diverse Image Priors Knowledge Distillation (DIP-KD) to address this problem. We first synthesize *image priors* — semantically diverse synthetic images, then further optimize them to a diversity objective via contrastive learning, and finally extract soft knowledge to distill the student. We achieve state-of-the-art KD performance for the black-box data-free settings on eight image benchmarks. This is backed by our deep analysis, showing that data diversity is effectively improved, and how it facilitates KD performance. We publish the source code at `https://osf.io/5mry8/?view_only=dee9e8fbcd114c34b45aa958a3aa32fa`.

1 Introduction

An inevitable side effect of advancing artificial intelligence (AI) that often gets overlooked is the sheer size of AI models. This obstacle limits their deployability in constrained environments, such as mobile or edge devices. Fortunately, research on model compression addresses this problem through various techniques such as model pruning, quantization, or low-rank factorization. Among these techniques, *knowledge distillation* (KD), proposed by Hinton et al. (2015), is well known for its efficiency and intuitive approach.

The intuition of KD closely resembles human learning: the knowledge is transferred from an expert network (*teacher*) to a novice network (*student*). In traditional machine learning, the student learns to predict the ground-truth labels from a dataset, much like a human learner does self-studying given a collection of exercises and solutions. KD advantageously supplements this learning process with the teacher's knowledge, which is more informative than the ground-truth labels. Thus, the student can reach comparable performance to the teacher, even when it may have a lesser capacity.

However, KD methods often require the teacher's original training data for optimal knowledge transfer. Nonetheless, such source datasets are often protected by stringent regulations as they are tied to security, privacy, and proprietary concerns. In fact, personal and health data, or data as intellectual properties all qualify for protection under the Database Directive (Directive 96/9/EC) and General Data Protection Regulation (GDPR) by European Parliament and Council (1996; 2016) in the EU, and under the Health Insurance Portability and Accountability Act (HIPAA) and the Data Security and Transparency Act (DSTA) by United States Congress (1996; 2016) in the US. These regulations effectively inhibit the use of traditional KD methods and pose the more challenging *data-free KD* problem.

Also crucial to KD is accessibility to the teacher model, varying from *white-box* — accessing the intermediate features, parameters, activations, or gradients (Romero et al., 2015; Yim et al., 2017; Chen et al., 2019) to *black-box* — only the final logits or predictive probabilities (Wang et al., 2020; Nguyen et al., 2022; Vo et al., 2024). Unfortunately, the teacher's accessibility is often restricted. For instance, proprietary large

language models, e.g., (OpenAI, 2025; Anthropic, 2025; xAI, 2025) return only textual replies instead of per-token scores. Similarly, certain evaluation servers, e.g., ImageNet by Russakovsky et al. (2015), only return the top-1 prediction, not class probabilities. Retrieving deeper insights via these interfaces is usually costly or even impossible. In conjunction, while *black-box data-free KD* (BBDFKD) is a realistic problem, its contraints invalidates most KD methods and calls for a fresh approach.

Without training data, previous methods utilize synthetic images to tackle BBDFKD. Yet, *diversity*, a pivotal factor for effective distillation, was under-investigated. ZSDB3 (Wang, 2021) samples synthetic images from random uniform noise and then updates them as trainable parameters. However, the synthetic images have a suboptimal initialization strategy, making them less diverse and some classes could be unforgivingly unobtainable. Differently, IDEAL (Zhang et al., 2022) and DFHL-RS (Yuan et al., 2024) leverage a generator network for synthetic images. Both attempted to generate class-balanced and realistic images, but were at risk of mode collapse caused by generator overfitting, as pointed out in Yuan et al. (2024). In addition, the majority of these methods are restricted to using a single index instead of probabilities as label during KD, affecting the student's learning.

Our method. We propose *Diverse Image Priors Knowledge Distillation* (**DIP-KD**) to tackle the BBDFKD problem, i.e., distilling the student from a black-box teacher which only returns top-1 prediction and without access to any real data. Focusing on data diversity, we realize our solution framework with three phases: *Synthesis*: to craft a pipeline of image priors with diverse distinct patterns, *Contrast*: to improve their diversity through contrastive learning, and *Distillation*: to train a high-performance student from these images.

Contribution. In summary, we highlight our contributions as follows:

1. We propose *image priors*, synthetic images crafted with diversity in hierarchical structures, nonlinearity, and meaningful semantics.
2. We investigate contrastive learning as a fitting strategy to improve image diversity, by making every images distinguishable.
3. We introduce a primer student to extract soft-probability as informative knowledge for KD, which is absent in previous BBDFKD methods.
4. Our analysis demonstrates our image priors are diverse in terms of both visuals and semantics, and show that they significantly contribute to KD performance.

2 Related Works

2.1 Knowledge Distillation

The pioneering idea in knowledge transferring from one neural network to another, intuitively, was to train the student to mimic the teacher's outputs (Bucilua et al., 2006). This idea was popularized in Hinton et al. (2015) as *knowledge distillation*, introducing the concept of *'soft'* probabilistic outputs, which are more informative than the *'hard'* class labels. Soft probabilities provide the student with *inter-class* relationships as hints for hidden knowledge, improving its performance. This foundational work has inspired a populated line of KD research: Romero et al. (2015); Chen et al. (2017); Park et al. (2019); Meng et al. (2019); Nguyen et al. (2021). Nonetheless, these methods are not effective for practical scenarios when data or model accessibility is limited.

2.2 Data-free Knowledge Distillation

The data availability hardship has inspired data-efficient KD approaches. While few-shot KD methods such as Wang et al. (2020); Nguyen et al. (2022); Vo et al. (2024) can reduce data requirements to a minimum, a small portion of the source dataset is still required. In practice, private datasets can be entirely closed, which will hinder these few-shot approaches. Some other approaches opt for using *proxy datasets* in the hope

they are exchangeable with the unknown source dataset (Chen et al., 2021; Tang et al., 2023). However, they often have a strong built-in bias that could mismatch with the teacher trained on a different dataset, as noted in Torralba & Efros (2011). When data access is prohibited, data-free KD approaches often rely on dissecting the teacher's internal structure or leveraging its gradients as guidance to harvest knowledge (Chen et al., 2019; Fang et al., 2019; 2021; Do et al., 2022; Tran et al., 2024).

2.3 Black-box Data-free Knowledge Distillation

Still, when the teacher model is black-box and has top-1 prediction only (i.e., with simple gradient-detaching and argmax operations), the data-free methods are challenged. The earliest to address BBDFKD is ZSDB3 by Wang (2021), which assumes: **(1)** the distance from an image sample to the decision boundary with other classes can represent its robustness, and **(2)** realistic images tend to be far away from these boundaries. This method uses random pixel-wise uniform noises for initialization and optimization. However, such high-dimensional boundaries can be over-complex for distance-based approaches, so the odds of obtaining diverse image samples are extremely slim and scale exponentially worse with high-resolution images or numerous classes. ZSDB3 was only successful in small-size, ten-class datasets.

Two subsequent works, IDEAL by Zhang et al. (2022) and DFHL-RS by Yuan et al. (2024), utilize an extra generator network for more flexible data generation. Both assume that as the student improves during KD, its gradients could guide generator training. The methods employ in-class similarity and class-balance objectives for the generator, which is popular in data-free KD (Chen et al., 2019). However, in black-box scenarios, while distilling an immature student is already challenging, its labels might not be reliable enough to guide generator training. This setup has been observed to cause *"overfitting of synthetic data"* to the student, resulting in possible mode collapse and insufficient diversity (Yuan et al., 2024).

3 Proposed Framework

Problem statement. Given solely a *black-box* pre-trained teacher network T that returns only top-1 hard labels and *no training data*, our goal is to train a student network S to approximate T.

Lacking a direct solution, we may tweak the standard KD framework (Hinton et al., 2015) as a naive solution. Without data, we may resort to using noise images, e.g., $x \sim \mathcal{X}_{\mathcal{U}}$, where $\mathcal{X}_{\mathcal{U}} = \mathcal{U}\left[0,1\right]^{C\times H\times W}$ and $C\times H\times W$ is the image dimension. Moreover, we can only use a hard label $\hat{y}_{T-\text{Hard}} = T(x) \in \{1,\dots,K\}$ to match the student's probabilistic outputs $\hat{y}_{S-\text{Soft}} = S\left(x\right)$ with the objective:

$$\mathcal{L}_{\text{Naive-KD}} = \mathbb{E}_{x\sim\mathcal{X}_{\mathcal{U}}}\left[\mathcal{L}_{\text{CE}}\left(\hat{y}_{S-\text{Soft}}, \hat{y}_{T-\text{Hard}}\right)\right], \tag{1}$$

where $\mathcal{L}_{\text{CE}}$ is the cross-entropy loss. While this approach can handle simple cases, it is apparent that it fails to use inter-class knowledge — the pivotal advantage in KD. Moreoever, we will show that noise images are semantically not diverse, and that diversity can drive KD performance through our proposed framework.

Proposal. To improve image diversity in BBDFKD, we propose *Diverse Image Priors Knowledge Distillation* (**DIP-KD**) of three phases: Synthesis, Contrast, and Distillation.

1. In the **Synthesis** phase, we design a pipeline to create *image priors* $\mathcal{X}_{\mathcal{P}}$ — synthetic images to capture diversity in hierarchical structures, nonlinearity, and meaningful semantics; which are often observed in natural scenes and objects. We achieve this via three sub-components: hierarchical noise, nonlinear transformation, and semantic cutmixing.

2. Then, in the **Contrast** phase, we sample a dataset $\mathcal{D} \coloneqq \{x | x \sim \mathcal{X}_{\mathcal{P}}\}$ and optimize them for diversity. We use a contrastive-based objective to make each and every sample *distinguishable*.

3. Finally, in the **Distillation** phase, we use $\mathcal{D}$ to distill the student S from the teacher T. Notably, we are able to extract logits from a primer student S_0 for soft knowledge to boost KD performance. This is absent in previous BBDFKD methods.

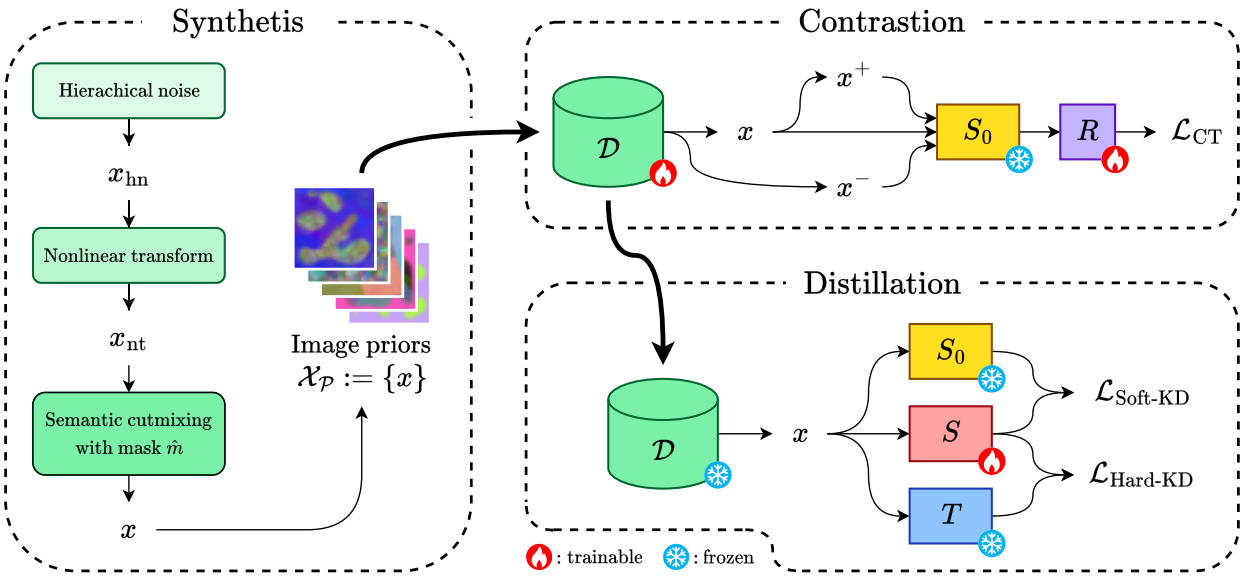

Figure 1: Illustration of our method **DIP-KD** of three phases. **(1) Synthesis:** To create image priors $\mathcal{X}_{\mathcal{P}}$, we create a pipeline of three sub-components: hierarchical noise, nonlinear transformation, and semantic cutmixing. Syntheic images $x \sim \mathcal{X}_{\mathcal{P}}$ have diverse and distinct patterns. **(2) Contrast:** We construct the dataset $\mathcal{D} := \{x | x \sim \mathcal{X}_{\mathcal{P}}\}$ to train an primer student S_0 as a feature extractor. Then, we enforce an instance-discriminator R to distinguish embeddings of images $x \sim \mathcal{D}$ to be similar to its positive view x^+, and dissimilar to its negative view $x^- \neq x$. Thus, $\mathcal{D}$ is optimized to be even more diverse. **(3) Distillation:** We distill the student S by matching with both hard labels from teacher T via $\mathcal{L}_{\text{Hard-KD}}$ and soft labels from primer student S_0 via $\mathcal{L}_{\text{Soft-KD}}$, providing extra knowledge.

3.1 Synthesis: crafting diverse image priors

From a visual recognition point-of-view, there exists *strong local structures* between neighbor pixels that compose *global patterns* in natural scenes and objects (LeCun et al., 1998). Moreover, natural objects usually consist of strong nonlinearity, and can capture complex semantics. Based on these premises, we create image priors $\mathcal{X}_{\mathcal{P}}$ with our Synthesis pipeline of three sub-components: *hierarchical noise*, *nonlinear transformation*, and *semantic cutmixing*. We showcase how diversity in image priors is enriched throughout the pipeline in Fig. 2, and will later examine their semantics in our analysis in Sec. 4.4.2.

3.1.1 Hierarchical noise

Hierarchy is an universal characteristic transcending natural scenes and objects. For instance, akin to how a vehicle is characterized by its windows, mirrors, wheels, an animal is easily recognizable via its eyes, ears, limbs. Based on this observation, we design a sampling technique that captures image patterns at both the local and global scales to mimic the *hierarchical structures* of visual signals.

For a pure pixel-wise noise image $x \sim \mathcal{X}_{\mathcal{U}} = \mathcal{U}[0,1]^{C \times H \times W}$, the patterns are majorly local and independent. Whereas, a monochromatic image (i.e., single-color) has dominant global correlation. Along this spectrum, there must exist a trade-off between the local-versus-global property. Inspiredly, we design a sampler composing noise images at multiple scales. Let us sample a collection of noise images with increasing dimensions until they sufficiently envelope $H \times W$:

$$\left\{ x_d | x_d \sim \mathcal{U}[0,1]^{C \times 2^d \times 2^d} \right\}_{d=0}^{d_{\max}}, \tag{2}$$

where $d_{\max} = \text{ceil}\left(\log_2 \max(H, W)\right)$ is the sufficient scale.

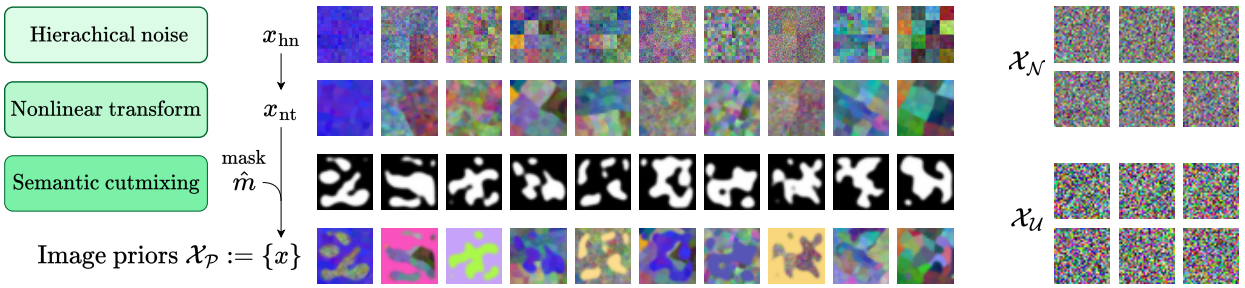

Figure 2: In the ***Synthesis*** phase, we generate image priors $\mathcal{X}_{\mathcal{P}}$ with 3 sub-components: **(1)** Hierchical noise: We sample x_{hn} from multi-scale noise images to capture hierarchical structures; **(2)** Nonlinear transform: We transform x_{hn} to x_{nt} with nonlinear filters to capture nonlinearity; and **(3)** Semantic cutmixing: We apply cutmixing on x_{nt} with a semantic mask $\hat{m}$ to construct the final images x, simulating diverse semantics. Observably, image priors $\mathcal{X}_{\mathcal{P}}$ have superior diversity to noise images sampled from random Gaussian distribution $\mathcal{X}_{\mathcal{N}}$ and random uniform distribution $\mathcal{X}_{\mathcal{U}}$.

Next, we aim to compose this collection of local-to-global noise to a single image. Thus, we proceed to sample coefficients $\{\alpha_d | \alpha_d \sim \mathcal{N}(0,1)\}_{d=0}^{d_{\max}}$ and put them through softmax to obtain each $\bar{\alpha}_d = \dfrac{\exp(\alpha_d)}{\sum_{d'=0}^{d_{\max}} \exp(\alpha_{d'})}$. This ensures $\sum_{d=0}^{d_{\max}} \bar{\alpha}_d = 1$ and $\bar{\alpha}_d \in [0,1]$ for a valid combination, which is our *hierarchical noise* image:

$$x_{\text{hn}} = \sum_{d=0}^{d_{\max}} \bar{\alpha}_d \cdot f_{\text{upscale}}\left(x_d; 2^{d_{\max}}\right), \tag{3}$$

where $f_{\text{upscale}}\left(\cdot; 2^{d_{\max}}\right)$ is an upscaling transformation so that noise images $\{x_d\}$ share equal dimensions to allow additivity.

3.1.2 Nonlinear transformation

To enrich nonlinear patterns of synthetic images, we apply random rotation f_{rot} of $[-45°, 45°]$, random elastic transform f_{elas}, and random cropping f_{crop} to the specified size $H \times W$. These operations are known to be nonlinear and effective in data augmentation (Simard et al., 2003), and in our case, boosting data diverity. Accordingly, we create a *nonlinear-transformed* image as:

$$x_{\text{nt}} = f_{\text{crop}}^{H \times W} \circ f_{\text{elas}} \circ f_{\text{rot}}^{[-45°, 45°]}(x_{\text{hn}}). \tag{4}$$

3.1.3 Semantic cutmixing

Finally, the semantics of natural objects usually consist of distinct cohesive shapes as the 'content', distinguishable to the background. Inspired by CutMix (Yun et al., 2019), we propose an improved masking technique to nonlinearly cutmix any two images together, creating diverse and semantically cohesive shapes.

We capture the semantics within a mask m, initialized to $m_0 \sim \mathcal{U}[0,1]^{1 \times H \times W}$. Regarding where $m < \beta$ as negative regions and $m \geq \beta$ as positive regions, the key to creating structurally cohesive shapes is to connect same-type regions but contrast opposite-type ones. While the former can be easily executed with a blurring filter f_{blur}, we design the diverging filter f_{divg} for images within the $[0,1]$ dynamic range as:

$$f_{\text{divg}}(m; 0 \leq \beta \leq 1) = \begin{cases} \frac{m^2}{\beta} & , m \geq \beta \\ \frac{m^2 - 2m + \beta}{\beta - 1} & , m < \beta \end{cases}. \tag{5}$$

We provide detailed formulation of f_{divg} in Appendix Sec. A.3.1. By design, f_{divg} is composed of two continuously differentiable half-parabolas: the left-side convex one on $[0, \beta)$, the right-side concave on $[\beta, 1]$, connected at the inflection point (β, β). To balance the divergence of the negative and positive regions,

we select $\beta = 0.5$. We iteratively pass the mask m_0 through the two filters as $m_{i+1} = f_{\text{blur}} \circ f_{\text{divg}}(m_i; \beta)$ (10 times) to obtain the final semantic mask $\hat{m}$. While our filters take care of creating cohesive shapes, the randomness in m_0 yields diverse $\hat{m}$. Based on $\hat{m}$, we pairwisely cut-mix $\{x_{\text{nt}}\}$ against themselves and random monochromatic images $\mathcal{X}_{\text{mc}} = \left\{ f_{\text{upscale}}^{H \times W}(x_{\text{mc}}) \,|\, x_{\text{mc}} \sim \mathcal{U}[0,1]^{C \times 1 \times 1} \right\}$ to form our final *image priors* $\mathcal{X}_{\mathcal{P}} \coloneqq \{x\}$, where:

$$x = \text{CutMix}(x_i, x_j; \hat{m} | x_i, x_j \sim \{x_{\text{nt}}\} \cup \mathcal{X}_{\text{mc}}; x_i \neq x_j). \tag{6}$$

3.2 Contrast: improving diversity via contrastive learning

We further improve the diversity of image priors $\mathcal{X}_{\mathcal{P}}$ through contrastive learning. However, contrastive methods usually requires extracting intermediate features, which is not feasible from a black-box teacher. Alternatively, we simply train a *primer* student S_0 on an image priors dataset $\mathcal{D} = \{x | x \sim \mathcal{X}_{\mathcal{P}}\}$. We also attempt to make $\mathcal{D}$ class-balanced via rejection sampling, which is efficient as $\mathcal{X}_{\mathcal{P}}$ is diverse. We train S_0 on $\mathcal{D}$ following the Hard-KD objective:

$$\mathcal{L}_{\text{Hard-KD}} = \mathbb{E}_{x \sim \mathcal{D}} \left[\mathcal{L}_{\text{CE}} \left(\hat{y}_{S_0 - \text{Soft}}, \hat{y}_{T - \text{Hard}} \right) \right], \tag{7}$$

where $\hat{y}_{S_0 - \text{Soft}} = S_0(x)$ is the probability prediction of the primer student, and $\hat{y}_{T-\text{Hard}} = T(x)$ is the hard label queried from the teacher. Equipped with a white-box S_0, we can explore its internal representations for contrastive learning.

Following Fang et al. (2021), diversity boils down to *"how distinguishable are the samples from the dataset"*. Interestingly, it can be explicitly formulated as an optimizable objective to mitigate the mode collapse and boost KD performance. For this goal, we utilize the primer student's backbone $S_0^{\mathcal{H}}$ to extract image embeddings and append an extra *instance-discriminator* R to treat each embedding as a distinct class. The network R is a shallow MLP (two linear layers) to project the general-purpose embeddings to a contrastive-specific space. We argue that even if S_0 might not have comparable performance to T, its backbone $S_0^{\mathcal{H}}$ can well capture the semantics, so R distinguishes them effectively. For any two images (x_i, x_j), we chain them through $S_0^{\mathcal{H}}$ and R to obtain their embeddings and quantify their cosine similarity as:

$$\text{Sim}(x_i, x_j) = \frac{\left\langle R \circ S_0^{\mathcal{H}}(x_i), R \circ S_0^{\mathcal{H}}(x_j) \right\rangle}{\left\| R \circ S_0^{\mathcal{H}}(x_i) \right\| \cdot \left\| R \circ S_0^{\mathcal{H}}(x_j) \right\|}. \tag{8}$$

To enforce contrastive learning, from an image $x \sim \mathcal{D}$, we create positive views x^+ with random augmentation and sample different images $x^- \sim \mathcal{D}$ (where $x^- \neq x$) as negative views. The contrastive loss is formulated to maximize the similarity between (x, x^+) and minimize that between (x, x^-):

$$\mathcal{L}_{\text{CT}} = \mathbb{E}_{x \sim \mathcal{D}} \left[-\log \frac{\exp(\text{Sim}(x, x^+))}{\sum_{x^- \neq x} \exp(\text{Sim}(x, x^-))} \right]. \tag{9}$$

We parameterized $\mathcal{D}$ and let the gradients of $\mathcal{L}_{\text{CT}}$ flow back to update a batch of $x \in \mathcal{D}$ and the instance-discriminator R at each time step. As the better R can learn to discriminate, the more distinguishable updates each $x \in \mathcal{D}$ can receive, and vice versa. This reinforcement effectively improves the diversity of $\mathcal{D}$.

3.3 Distillation: Training the student network

After $\mathcal{D}$ has been optimized for diveristy, we use them to distill the student S. We aim to encorporate both *hard* and *soft* knowledge, which is **fundamental** in KD (Hinton et al., 2015), to construct an *optimal* distillation objective. This is either *limited* or *entirely absent* in Wang (2021); Zhang et al. (2022); Yuan et al. (2024). Contrarily, having privilege access to the primer network S_0, we can jointly match our student's logits $S^{\mathcal{Z}}(x)$ with logits of the primer student $S_0^{\mathcal{Z}}(x)$ as soft labels, and with queries $\hat{y}_{T-\text{Hard}}$ from the teacher T as hard labels:

$$\mathcal{L}_S = \mathcal{L}_{\text{Hard-KD}} + \mathcal{L}_{\text{Soft-KD}} = \mathbb{E}_{x \sim \mathcal{D}} \Big[\mathcal{L}_{\text{CE}} \left(\hat{y}_{S - \text{Soft}}, \hat{y}_{T - \text{Hard}} \right) + \mathcal{L}_{\text{L1}} \left(S^{\mathcal{Z}}(x), S_0^{\mathcal{Z}}(x) \right) \Big], \tag{10}$$

where $\mathcal{L}_{\text{L1}}$ is the L1 divergence loss that captures the privilege inter-class knowledge. To conclude our framework, we summarize it as pseudocode in Alg. 1.

Algorithm 1: Proposed method **DIP-KD**

Input: a pre-trained teacher network T
Parameters: number of synthetic images N
Output: a student network S

▷ ***Synthesis***
Construct hierarchical noise images $\{x_{\text{hn}}\}$ via Eq. 2, 3
Apply nonlinear transforms on $\{x_{\text{nt}}\}$ to obtain $\{x_{\text{hn}}\}$ via Eq. 4
Apply semantic cutmixing on $\{x_{\text{hn}}\}$ to obtain $\mathcal{X}_{\mathcal{P}} \coloneqq \{x\}$ via Eq. 5, 6

▷ ***Contrast***
Construct and parameterize dataset $\mathcal{D} = \{x | x \sim \mathcal{X}_{\mathcal{P}}\}_{i=1}^{N}$
Train primer student S_0 by querying T on $\mathcal{D}$ to minimize $\mathcal{L}_{\text{Hard-KD}}$ via Eq. 7
Initialize instance-discriminator R
while *($\mathcal{D}$ not converged)* **do**
    Sample $x \sim \mathcal{D}$ and their positive x^+ and negative views $x^- \neq x$
    Update x and R to minimize $\mathcal{L}_{\text{CT}}$ via Eq. 9

▷ ***Distillation***
Distill student S by querying T and S_0 on $\mathcal{D}$ to minimize via $\mathcal{L}_S$ Eq. 10

return S

4 Experiments

To demonstrate the effectiveness of our method DIP-KD, we evaluated our method on extensive BBDFKD benchmarks. Furthermore, we conduct a wide range of ablation studies and analysis to reveal the underlying mechanics of our framework, and validate it under practical scenarios. We also provide training details, complementary studies, and extended works in the Appendix.

4.1 Experimental setup

We evaluate our method across eight benchmark datasets at various difficulty: MNIST (LeCun et al., 1998), USPS (Hull, 1994), SVHN (Netzer et al., 2011), FMNIST (Xiao et al., 2017), CIFAR10, CIFAR100 (Krizhevsky et al., 2009), Tiny-ImageNet (Le & Yang, 2015) (abbreviated: TinyImageNet), Imagenette (FastAI, 2020). Three network architectures are considered for the teacher and student, namely LeNet5 (LeCun et al., 1998), AlexNet (Krizhevsky et al., 2012), and ResNet (He et al., 2016). These datasets and architectures are the de facto evaluation in BBDFKD methods (Wang, 2021; Zhang et al., 2022; Yuan et al., 2024). For detailed training setups, we kindly refer readers to Appendix Sec. A.

4.2 Baselines

We compare our method DIP-KD with the baselines:

- Naive-KD: The student is trained on uniform noise $x \sim \mathcal{X}_{\mathcal{U}}$, where $\mathcal{X}_{\mathcal{U}} = \mathcal{U}\,[0,1]^{C\times H\times W}$ and the teacher's hard labels $\hat{y}_{T-\text{Hard}} = T\,(x) \in \{1,\ldots,K\}$.
- BBDFKD methods: We compare ours with three state-of-the-art methods: ZSDB3 (Wang, 2021), IDEAL (Zhang et al., 2022), and DFHL-RS (Yuan et al., 2024).

For fair comparisons and where applicable, we used the same/smaller teacher-student network architectures and the same/smaller numbers of synthetic images as in the baseline methods. We report the *mean* ± *standard error* of distillation accuracy, which is student's accuracy on the hold-out test set, across five runs. The accuracy of baseline BBDFKD methods are obtained from their respective publications.

4.3 Standard experiments

We categorize the datasets into simple and complex datasets based on their difficulty. Four simple datasets MNIST, USPS, SVHN, FMNIST all have 10 classes of simple objects, at a 32×32 or smaller resolution. The complex datasets have more complicated objects or more classes: CIFAR10 and CIFAR100 (10 and 100 classes, 32×32), TinyImageNet (200 classes, 64×64), and Imagenette (10 classes, but high-resolution). More details on the dataset can be found in Appendix Sec. A.1.

Table 1: Distillation accuracy (%) on simple datasets.

Baseline	**MNIST** LeNet5 $N = 20$ K	**USPS** LeNet5 $N = 50$ K	**SVHN** AlexNet $N = 50$ K	**FMNIST** LeNet5 $N = 50$ K
Teacher	99.28	95.47	96.16	90.90
Naive-KD	$96.54_{\pm.60}$	$42.05_{\pm.08}$	$83.35_{\pm.57}$	$55.11_{\pm1.23}$
ZSDB3	$96.54^{[4\times]}$	-	-	$72.31^{[1.6\times]}$
IDEAL	$96.32^{[1.3\times]}$	-	$84.42^{[2\times]}$	$83.92^{[2\times]}$
DIP-KD	$\mathbf{98.59}_{\pm.08}$	$\mathbf{94.20}_{\pm.21}$	$\mathbf{95.94}_{\pm.05}$	$\mathbf{83.98}_{\pm\ .65}$

N: synthetic dataset size; Subscript $_{\pm\ldots}$ denotes the standard error; Bracketed superscript $^{[\ldots\times]}$ denotes how much more data the baseline requires; Best results are in **bold**.

Simple datasets. We report knowledge distillation (KD) results on simple datasets in Table 1. Across all cases, BBDFKD baselines consistently outperform Naive-KD. DFHL-RS did not experiment with these benchmarks, questioning its peformance on small-scale settings. Notably, our proposed method, DIP-KD, surpasses all BBDFKD baselines despite relying on the smallest amount of synthetic data. This demonstrates the effectiveness of DIP-KD to achieve superior distillation performance.

Table 2: Distillation accuracy (%) on complex datasets.

Baseline	**CIFAR10** ResNet18 $N = 50$K	**CIFAR100** ResNet18 $N = 100$K	**TinyImageNet** ResNet18 $N = 512$K	**Imagenette** ResNet18 $N = 50$K
Teacher	95.21	78.36	66.08	91.29
Naive-KD	$13.99_{\pm.23}$	$2.68_{\pm.13}$	$0.75_{\pm.07}$	$33.21_{\pm\ .39}$
ZSDB3	$59.46^{[1.6\times]}$	-	-	-
IDEAL	$68.82^{[5\times]}$	$36.96^{[20\times]}$	$27.95^{[3.9\times]}$	-
DFHL-RS	$77.86^{[2.6\times]}$	$51.94^{[2.6\times]}$	-	-
DIP-KD	$\mathbf{83.41}_{\pm.46}$	$\mathbf{52.85}_{\pm.30}$	$\mathbf{28.03}_{\pm.22}$	$\mathbf{61.84}_{\pm0.77}$

N: synthetic dataset size; Subscript $_{\pm\ldots}$ denotes the standard error; Bracketed superscript $^{[\ldots\times]}$ denotes how much more data the baseline requires; Best results are in **bold**.

Complex datasets. For complex datasets, we summarized distillation performance in Table 2. Naive-KD exhibits a catastrophic performance drop to near random-guessing levels, due to the limited diversity in its training data $\mathcal{X}_{\mathcal{U}}$. Sampling from $\mathcal{X}_{\mathcal{U}}$ saturates at only 5/100 and 6/200 classes on CIFAR100 and TinyImageNetet, respectively, highlighting the difficulty of these datasets. We also observed the relative performance gap between DIP-KD and other baselines to be even wider compared to that on simple datasets in Table 1, indicating that DIP-KD maintains robustness under challenging conditions. Furthermore, we are the first BBDFKD method to evaluate on high-resolution images, achieving a moderate accuracy of 62.78% on Imagenette. Based on these results, we believe DIP-KD show great potential in practical applications.

4.4 Ablation studies

In this section, we provide deeper insights into our framework by dissecting the components of our framework, and then put it to practical settings. Formerly, we perform an analysis on individual component's contribution, explore the semantics and visualization of our image priors, and examine our method's sensitivity to hyperparameters. Then, we extend our evaluation to real-world scenarios such as KD with proxy data, with cross-architecture settings, or under aggressive model compression. We also refer enthusiastic readers to visit Appendix Sec. B for complementary studies on alternative optimization objectives, and Appendix Sec. C for an iterative extension of our method.

4.4.1 Contribution of components

Table 3: Distillation accuracy (%) by inclusion of components.

Method	MNIST	CIFAR10
Naive-KD (noise data $x \sim \mathcal{X}_{\mathcal{U}}$, hard labels)	$96.02_{\pm.60}$	$13.99_{\pm.23}$
+ **Synthesis:**	+ 2.27	+ 64.18
▲Hierarchical noise: $\mathcal{D} \coloneqq \{x_{\text{hn}}\}$	1.79▲	59.26▲
▲Nonlinear transform: $\mathcal{D} \coloneqq \{x_{\text{nt}}\}$	0.18▲	2.38▲
▲Semantic cutmixing: $\mathcal{D} \coloneqq \{x \mid x \sim \mathcal{X}_{\mathcal{P}}\}$	0.30▲	2.54▲
+ **Contrast:** Update $\mathcal{D}$ to minimize $\mathcal{L}_{\text{CT}}$ via Eq. 9	+ 0.16	+ 3.14
+ **Distillation:** Add Soft-KD to $\mathcal{L}_S$ in Eq. 10	+ 0.14	+ 2.10
Complete **DIP-KD**	$98.59_{\pm.08}$	$83.41_{\pm.46}$

▲ denotes individual contribution of each Synthesis sub-components.
Subscript $_{\pm\ldots}$ denotes the standard error at the base and complete case.

We investigate each component of our framework DIP-KD on MNIST and CIFAR10 from the standard experiment, as representative for simple and complex benchmarks. Starting from the baseline Naive-KD, we sequentially add each component and report the student accuracy in Table 3. Firstly, Synthesis contributes the most to student accuracy (+2.27% on MNIST, +64.18% on CIFAR10), where the hierarchical noise sub-component has the most impact. Other components further improve the student, more apparently on CIFAR10 thanks to its relative difficulty, i.e., +3.14% for Contrast and +2.10% for Distillation. This confirms Synthesis and Contrast can initialize and optimize synthetic data with *diversity*, and Distillation can transfer their inter-class knowledge to the student.

4.4.2 Embeddings analysis — Generation

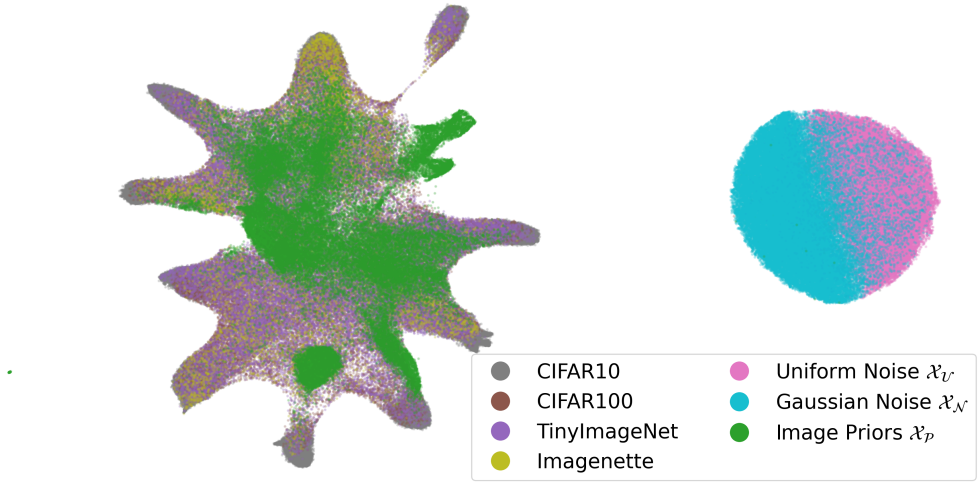

Figure 3: Feature embeddings of complex datasets, noise ($\mathcal{X}_{\mathcal{U}}$, $\mathcal{X}_{\mathcal{N}}$), and image priors $\mathcal{X}_{\mathcal{P}}$.

To ensure that our image priors are diverse and semantically meaningful, we sample random synthetic images and extract their embeddings from the backbone of the ResNet18 teacher network pre-trained on CIFAR10. Its intermediate features have a dimension of 512, where we further embed with UMAP (McInnes et al., 2018) with default parameters to two-dimensional for visualization. We explore four complex datasets CIFAR10, CIFAR100, TinyImageNet, and Imagenette, which contain rich diversity and semantics. We also include uniform noise $\mathcal{X}_{\mathcal{U}}$, Gaussian noise $\mathcal{X}_{\mathcal{N}}$, and our image priors $\mathcal{X}_{\mathcal{P}}$. We visualize these embeddings in Fig. 3 for a qualitative study.

Apparently, $\mathcal{X}_{\mathcal{U}}$ and $\mathcal{X}_{\mathcal{N}}$ form a compact, separate cluster far away from the regions of real images, suggesting that their semantics are limited and dissimilar to natural objects. In contrast, $\mathcal{X}_{\mathcal{P}}$ widely spreads among the mutual regions of real images, hinting that they share similar semantics as expected. For quantitative analysis, we evaluate four distribution metrics for generative models from Naeem et al. (2020):

- *Precision*: the fraction of synthetic samples that is in the neighborhood of at least one real sample. High precision indicates synthetic data are captured within the support of real data, but may be *biased* by real outlier samples.
- *Recall*: the fraction of real samples that is in the neighborhood of at least one synthetic sample. High recall indicates synthetic data can capture the support of real data, but may be *biased* by an overestimated synthetic manifold.
- *Density*: the average normalized count of synthetic samples in the neighborhood of each real sample. High density indicates *fidelity* like precision but is less *biased*, and may be greater than 1 when synthetic data concentrates around real modes.
- *Coverage*: the fraction of real samples whose neighbourhoods contain at least one fake sample. High coverage indicates *diversity* like recall but is less *biased*.

Table 4: Distribution metrics (%) on complex datasets.

Metric	Source	CIFAR10	CIFAR100	TinyImageNet	Imagenette
Density	$\mathcal{X}_{\mathcal{U}}$	20.00	100.65	108.65	101.20
	$\mathcal{X}_{\mathcal{N}}$	20.00	107.98	90.87	103.64
	$\mathcal{X}_{\mathcal{P}}$	49.14	96.20	96.00	92.14
Coverage	$\mathcal{X}_{\mathcal{U}}$	.00	.10	.06	.05
	$\mathcal{X}_{\mathcal{N}}$	.00	.10	.06	.05
	$\mathcal{X}_{\mathcal{P}}$	7.33	60.79	63.88	78.48
Precision	$\mathcal{X}_{\mathcal{U}}$	100.00	100.10	100.00	100.00
	$\mathcal{X}_{\mathcal{N}}$	100.00	100.10	100.00	100.00
	$\mathcal{X}_{\mathcal{P}}$	80.83	97.76	99.29	99.10
Recall	$\mathcal{X}_{\mathcal{U}}$	.00	.09	.06	.04
	$\mathcal{X}_{\mathcal{N}}$	.00	.10	.06	.05
	$\mathcal{X}_{\mathcal{P}}$	66.92	96.75	96.86	95.07

The statistics in Table 4 shows that our image priors $\mathcal{X}_{\mathcal{P}}$ achieved significantly higher density, coverage, and recall at a small trade-off in precision, compared to noise sources $\mathcal{X}_{\mathcal{U}}$ and $\mathcal{X}_{\mathcal{N}}$. Theses results further confirm $\mathcal{X}_{\mathcal{P}}$ have superior fidelity and diversity, and explains why $\mathcal{X}_{\mathcal{P}}$ excels in BBDFKD.

4.4.3 Embeddings analysis — Contrast

To highlight the effect of the Contrast phase on increasing diversity of image priors, we visualize the embeddings of 50K images before and after the Contrast phase in Fig. 4. Embeddings are extracted similarly as previously described, using the ResNet18 backbone pre-trained on CIFAR10. The backbone can proficiently recognize the semantics and embed real images into ten distinctive clusters (colored gray). Image priors $\mathcal{X}_{\mathcal{P}}$

before Contrast (green) already scatter around these clusters, indicating they have captured diverse semantics. After Contrast, the contrastive objective further improves the coverage and expands $\mathcal{X}_{\mathcal{P}}$ to neighbor regions as well (orange).

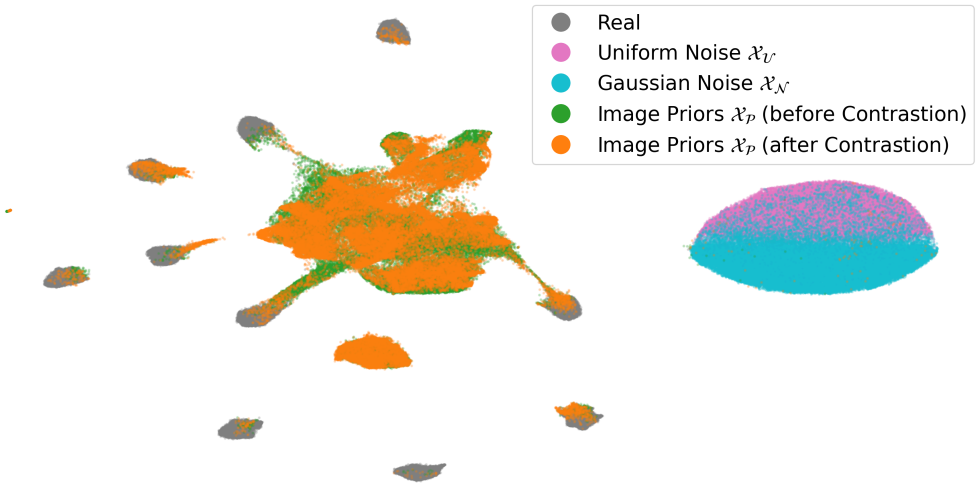

Figure 4: Feature embeddings of image priors $\mathcal{X}_{\mathcal{P}}$ on CIFAR10 before and after the Contrast step, with real data and noise sources.

Upon closer inspection of randomly-picked image priors (Fig. 5), we observe that the contrastive optimization has overlay the image priors with faint but self-distinguished patterns after Contrast. In most images, the residual can be seen to reinforce the existing patterns. We also observe a significant increase in density, coverage, and recall, with a trivial trade-off in density (Table 5). Overall, these results show that the Contrast phase improve image diversity semantically, visually, and empirically.

(a) Before Contrast

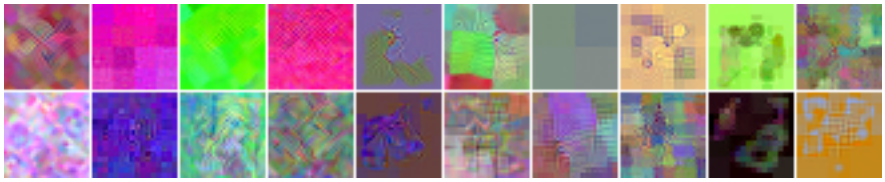

(b) After Contrast

Figure 5: Contrastive optimization to image priors $\mathcal{X}_{\mathcal{P}}$ during the Contrast phase.

Table 5: Distribution metrics (%) during the Contrast phase.

	Density	**Coverage**	**Precision**	**Recall**
Before Contrast	70.46	6.13	91.69	82.18
After Contrast	66.93	14.66	91.68	94.00

4.4.4 Increasing synthetic dataset size

While it is unsurprising that we achieved better KD performance when using more a larger number of image priors N (Fig. 6), more important discussions are: which is the optimal cut-off point, and how it corresponds to the relative difficulty of each dataset. We observe that for the digits datasets (MNIST, UPSP, SVHN), the student fits easily even with minimal data ($N = 10$K), whereas it struggles a bit more on FMNIST and CIFAR10. For CIFAR100, TinyImageNet, and Imagenette, the student still stably improves even after we have reached $N = 100$K or more, suggesting that increasing N is a viable option for large-scale problems.

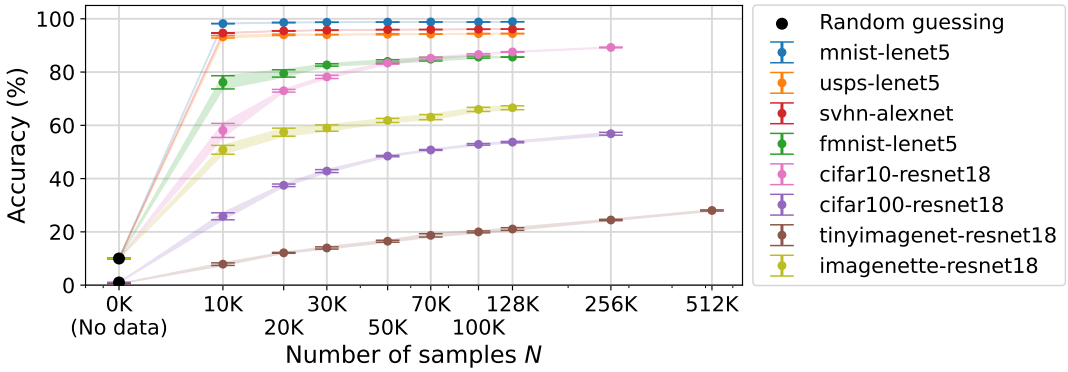

Figure 6: Distillation accuracy (%) by number of image priors N.

4.4.5 Distilling with proxy data

Thanks to the digits datasets (MNIST, UPSP, SVHN) having shared classes (digits 0–9), we also explore using out-of-domain datasets as proxy data as another naive approach. We evaluate students trained with different combinations of input images (real training sets, noises, and our image priors) and labels (ground truth from real training sets, or pseudo-labels given by the teacher). We use 50K images for each synthetic source, and the full training set for each real dataset. For fair comparisons, we only include the *Synthesis* component (i.e., accuracy of primer student S_0) for our method, and reuse the teachers from standard experiments. We also emphasize that using real training sets containing shared classes is *unfair* to our data-free premise, which starts with strictly no data.

Table 6: Distillation accuracy (%) with proxy data.

Training data		**Evaluation**		
Inputs	**Labels**	**MNIST** LeNet5	**USPS** LeNet5	**SVHN** AlexNet
MNIST	ground-truth	**99.25**$_{\pm .06}$	91.88$_{\pm 1.56}$	20.77$_{\pm .29}$
	pseudo	**99.06**$_{\pm .05}$	93.94$_{\pm .30}$	41.18$_{\pm 3.27}$
USPS	ground-truth	77.92$_{\pm 2.72}$	**95.90**$_{\pm .48}$	19.36$_{\pm .62}$
	pseudo	96.78$_{\pm .42}$	**94.97**$_{\pm .15}$	57.52$_{\pm 1.81}$
SVHN	ground-truth	64.10$_{\pm 1.29}$	62.12$_{\pm 1.68}$	**95.97**$_{\pm .08}$
	pseudo	98.59$_{\pm .18}$	93.95$_{\pm .37}$	**96.48**$_{\pm .04}$
$\mathcal{X}_\mathcal{N}$	pseudo	88.05$_{\pm .76}$	27.29$_{\pm .10}$	84.42$_{\pm .48}$
$\mathcal{X}_\mathcal{U}$		96.54$_{\pm .60}$	42.05$_{\pm .08}$	83.35$_{\pm .57}$
$\mathcal{X}_\mathcal{P}$		**98.62**$_{\pm .17}$	**94.14**$_{\pm .52}$	**95.84**$_{\pm .10}$

Subscript $_{\pm ...}$ denotes the standard error.
The top-3 results from each target evaluation (column) are in **bold**.

We adopt the perspective of domain adaptation theory in Ben-David et al. (2010) to discuss our results summarized in Table 6.

- First, when the teacher's original training set is available—representing an in-domain scenario—the student model achieves the highest performance. This outcome is expected, as having access to an identical curriculum allows the student to mimic the teacher most effectively.
- Second, performing knowledge distillation in an adaptation-like manner (e.g., from MNIST to USPS) by querying the teacher on proxy datasets provides only a modest improvement over using drop-in labels. Despite the availability of high-quality images, this approach **fails** to achieve satisfactory performance. We hypothesize that this limitation is caused by the domain gap between the teacher's knowledge and the foreign data. Hence, employing public datasets as direct proxies may, in fact, degrade KD performance.
- Finally, rather than *exploitation* over an *uncertain* domain, it is more advantageous to prioritize *exploration* over a *diverse* domain, especially in the BBDFKD setting. Evidently, our results with image priors $\mathcal{X}_{\mathcal{P}}$ (bottom row) approximates the in-domain settings with less than a 1% difference.

Collectively, these insights indicate our image priors exhibits a *universal* diversity and broad applicablity.

4.4.6 Cross-architecture KD

An under-investigated setting in BBDFKD methods is distilling from the teacher to students of heterogeneous architecture. To fully discriminate the knowledge gap, we evaluate three architectures with large capacity difference: LeNet5, AlexNet, and ResNet18; on three benchmarks with intermediate difficulty: FMNIST, SVHN, and CIFAR10. We reuse the same teacher networks from the standard experiments and report the KD results in Table 7. On the diagonal, we observe that the student performs best when it has a homogeneous architecture to the teacher. Otherwise, accuracy scales with capacity, and a medium-size student can still often give moderate results. Thus, DIP-KD is proven to be applicable even when the teacher and student may have different architectures.

Table 7: Distillation accuracy (%) of cross-architecture KD.

Network	**FMNIST** LeNet5	**SVHN** AlexNet	**CIFAR10** ResNet18
Teacher	90.90	96.16	95.21
LeNet5	**83.98**$_{\pm\ .65}$	64.44$_{\pm 1.83}$	32.01$_{\pm 3.18}$
AlexNet	78.98$_{\pm\ .92}$	**95.94**$_{\pm\ .05}$	61.30$_{\pm 0.69}$
ResNet18	81.69$_{\pm 1.58}$	95.91$_{\pm\ .04}$	**83.41**$_{\pm\ .46}$

Subscript $_{\pm \ldots}$ denotes the standard error.
Best results are in **bold**.

4.4.7 Students of compressed capacity

While we used same-size teacher-student networks in the standard experiment for fair comparision, we are also interested in the case when the student gets aggressively compressed, which has yet to be investigated in previous methods. Specifically, we train on student networks of approximately 25%, 4%, and 1% compression ratio (CR) by reducing the number of channels in linear and convolutional layers by 2×, 5×, 10×, respectively (Table 8). We distill these compressed students using our method, while keeping all other settings the same as in the standard experiments.

Table 8: Parameters count by compression ratio (CR).

CR	**LeNet5**	**AlexNet**	**ResNet18**
100%	61.71 K	1,659.18 K	11.17 M
50%	15.74 K	417.43 K	2.90 M
20%	2.53 K	68.49 K	0.45 M
10%	0.88 K	17.70 K	0.11 M

We report the KD results in Fig. 7 and observe that our method is empirically robust to moderate compression. Even at 25% CR, the students are mostly unaffected across all datasets, and only suffer a tolerable decline in accuracy around 4% CR. Only at the extreme 1% CR, the students starts to decline significantly. This encouraging result shows that DIP-KD is effective in distilling a cumbersome teacher into lightweight students, which is particularly useful for *resource-constrained* settings, such as mobile or edge devices.

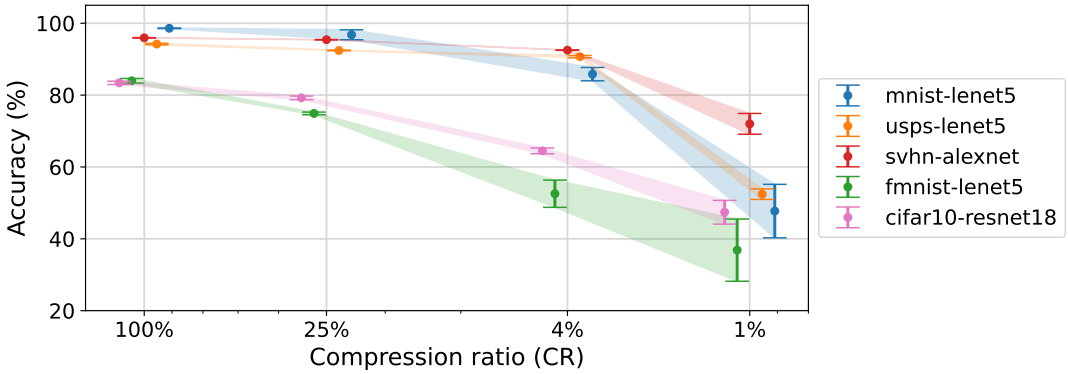

Figure 7: Distillation accuracy (%) by compression ratio (CR).

5 Ethical considerations

Our study explores *black-box data-free knowledge distillation*, a setting where a student model learns from a teacher's outputs without access to its internal parameters or original training data. While not apparent, we would like to raise certain ethical and societal concerns related to model extraction and information leakage.

Because the student learns entirely from the teacher's responses, repeated querying could approximate the teacher's decision boundaries, potentially enabling unauthorized reconstruction of proprietary or commercial models (Tramer et al., 2016; Orekondy et al., 2019; Jagielski et al., 2020). Large-scale replication of closed models could discourage openness in AI research and reduce incentives for model providers to offer public APIs. This problem could be mitigated by limiting the queries to the teacher, and through model watermarking or output perturbation that make functional copying more detectable or less precise (Jia et al., 2021; Wang et al., 2024).

Besides, even though no real data are used, teacher models may implicitly memorize sensitive information that can be exposed through their responses (Carlini et al., 2021). In extreme cases, this could lead to indirect leakage of personal or confidential data. Such leakage risks eroding public trust in machine learning systems and may breach data protection norms if human-derived models are involved. As a recommendation, using privacy-preserving training techniques, such as differential privacy (Flemings & Annavaram, 2024), and conducting ethical audits of teacher outputs can reduce the likelihood of revealing sensitive patterns.

Our aim is to enable ethical and resource-efficient research on knowledge distillation, not to facilitate extraction or imitation of closed systems. We therefore restrict our experiments to openly licensed teacher models and open-source our works to encourage transparent, auditable research practices.

6 Conclusion

While most knowledge distillation techniques can train competent students, they often struggle in real-world settings where access to the original training data and teacher network is limited. To bridge this gap, we introduce DIP-KD, a novel framework for data-free knowledge distillation from a black-box teacher. Our framework synthesizes diverse images through a tailored generation pipeline, enhance their distinction via contrastive learning, and distill a student using both hard and soft knowledge. We achieve state-of-the-art results on eight benchmarks and deliver comprehensive analyses and experiments. We hope this work not only solves a non-trivial KD problem but also sparks new directions and challenges for future KD research.

References

Anthropic. Introducing claude sonnet 4.5, 2025. URL https://www.anthropic.com/news/claude-sonnet-4-5.

Shai Ben-David, John Blitzer, Koby Crammer, Alex Kulesza, Fernando Pereira, and Jennifer Wortman Vaughan. A theory of learning from different domains. *Machine learning*, 79:151–175, 2010.

Cristian Bucilua, Rich Caruana, and Alexandru Niculescu-Mizil. Model compression. In *KDD*, 2006.

Nicholas Carlini, Florian Tramer, Eric Wallace, Matthew Jagielski, Ariel Herbert-Voss, Katherine Lee, Adam Roberts, Tom Brown, Dawn Song, Ulfar Erlingsson, et al. Extracting training data from large language models. In *USENIX*, pp. 2633–2650, 2021.

Guobin Chen, Wongun Choi, Xiang Yu, Tony Han, and Manmohan Chandraker. Learning efficient object detection models with knowledge distillation. *NeurIPS*, 30, 2017.

Hanting Chen, Yunhe Wang, Chang Xu, Zhaohui Yang, Chuanjian Liu, Boxin Shi, Chunjing Xu, Chao Xu, and Qi Tian. Data-free learning of student networks. In *ICCV*, 2019.

Hanting Chen, Tianyu Guo, Chang Xu, Wenshuo Li, Chunjing Xu, Chao Xu, and Yunhe Wang. Learning student networks in the wild. In *CVPR*, 2021.

Kien Do, Thai Hung Le, Dung Nguyen, Dang Nguyen, Haripriya Harikumar, Truyen Tran, Santu Rana, and Svetha Venkatesh. Momentum adversarial distillation: Handling large distribution shifts in data-free knowledge distillation. *NeurIPS*, 35, 2022.

European Parliament and Council. Directive 96/9/ec of the european parliament and of the council of 11 march 1996 on the legal protection of databases. *Official Journal of the European Communities*, L 77, 20–28, 1996. URL https://eur-lex.europa.eu/legal-content/EN/TXT/?uri=celex%3A31996L0009. Adopted 11 March 1996, published 27 March 1996.

European Parliament and Council. Regulation (eu) 2016/679 of the european parliament and of the council of 27 april 2016 on the protection of natural persons with regard to the processing of personal data and on the free movement of such data (general data protection regulation). *Official Journal of the European Union*, L 119, 1–88, 2016. URL https://eur-lex.europa.eu/legal-content/EN/TXT/?uri=CELEX%3A32016R0679. Adopted 27 April 2016, entered into force 25 May 2018.

Gongfan Fang, Jie Song, Chengchao Shen, Xinchao Wang, Da Chen, and Mingli Song. Data-free adversarial distillation. *arXiv:1912.11006*, 2019.

Gongfan Fang, Jie Song, Xinchao Wang, Chengchao Shen, Xingen Wang, and Mingli Song. Contrastive model inversion for data-free knowledge distillation. In *IJCAI*, 2021.

FastAI. Imagenette. GitHub, 2020. URL https://github.com/fastai/imagenette.

James Flemings and Murali Annavaram. Differentially private knowledge distillation via synthetic text generation. *ACL Findings*, 2024.

Kaiming He, Xiangyu Zhang, Shaoqing Ren, and Jian Sun. Deep residual learning for image recognition. In *CVPR*, 2016.

Geoffrey Hinton, Oriol Vinyals, and Jeff Dean. Distilling the knowledge in a neural network. *arXiv:1503.02531*, 2015.

Jonathan J. Hull. A database for handwritten text recognition research. *PAMI*, 1994.

Matthew Jagielski, Nicholas Carlini, David Berthelot, Alex Kurakin, and Nicolas Papernot. High accuracy and high fidelity extraction of neural networks. In *USENIX*, pp. 1345–1362, 2020.

Hengrui Jia, Christopher A Choquette-Choo, Varun Chandrasekaran, and Nicolas Papernot. Entangled watermarks as a defense against model extraction. In *USENIX*, pp. 1937–1954, 2021.

Diederik P Kingma and Jimmy Ba. Adam: A method for stochastic optimization. *arXiv:1412.6980*, 2014.

Alex Krizhevsky, Geoffrey Hinton, et al. Learning multiple layers of features from tiny images. Technical report, University of Toronto, 2009.

Alex Krizhevsky, Ilya Sutskever, and Geoffrey E Hinton. Imagenet classification with deep convolutional neural networks. *NeurIPS*, 25, 2012.

Yann Le and Xuan Yang. Tiny ImageNet visual recognition challenge. *CS 231N*, 2015.

Yann LeCun, Leon Bottou, Yoshua Bengio, and Patrick Haffner. Gradient-based learning applied to document recognition. *Proceedings of the IEEE*, 1998.

Leland McInnes, John Healy, and James Melville. Umap: Uniform manifold approximation and projection for dimension reduction. *arXiv:1802.03426*, 2018.

Zhong Meng, Jinyu Li, Yong Zhao, and Yifan Gong. Conditional teacher-student learning. In *ICASSP*. IEEE, 2019.

Muhammad Ferjad Naeem, Seong Joon Oh, Youngjung Uh, Yunjey Choi, and Jaejun Yoo. Reliable fidelity and diversity metrics for generative models. In *ICML*, pp. 7176–7185. PMLR, 2020.

Yuval Netzer, Tao Wang, Adam Coates, Alessandro Bissacco, Baolin Wu, Andrew Y Ng, et al. Reading digits in natural images with unsupervised feature learning. In *NeurIPS*. Granada, 2011.

Dang Nguyen, Sunil Gupta, Trong Nguyen, Santu Rana, Phuoc Nguyen, Truyen Tran, Ky Le, Shannon Ryan, and Svetha Venkatesh. Knowledge distillation with distribution mismatch. In *ECML-PKDD*. Springer, 2021.

Dang Nguyen, Sunil Gupta, Kien Do, and Svetha Venkatesh. Black-box fewshot knowledge distillation. In *ECCV*, 2022. doi: 10.1007/978-3-031-19803-8_12.

OpenAI. Introducing gpt-5, 2025. URL `https://openai.com/index/introducing-gpt-5`.

Tribhuvanesh Orekondy, Bernt Schiele, and Mario Fritz. Knockoff nets: Stealing functionality of black-box models. In *CVPR*, pp. 4954–4963, 2019.

Wonpyo Park, Dongju Kim, Yan Lu, and Minsu Cho. Relational knowledge distillation. In *CVPR*, pp. 3967–3976, 2019.

Adriana Romero, Nicolas Ballas, Samira Ebrahimi Kahou, Antoine Chassang, Carlo Gatta, and Yoshua Bengio. Fitnets: Hints for thin deep nets. *ICLR*, 2015.

Olga Russakovsky, Jia Deng, Hao Su, Jonathan Krause, Sanjeev Satheesh, Sean Ma, Zhiheng Huang, Andrej Karpathy, Aditya Khosla, Michael Bernstein, et al. Imagenet large scale visual recognition challenge. *IJCV*, 115, 2015.

Patrice Y Simard, David Steinkraus, John C Platt, et al. Best practices for convolutional neural networks applied to visual document analysis. In *ICDAR*, volume 3. Edinburgh, 2003.

Jialiang Tang, Shuo Chen, Gang Niu, Masashi Sugiyama, and Chen Gong. Distribution shift matters for knowledge distillation with webly collected images. In *ICCV*, 2023.

Antonio Torralba and Alexei A Efros. Unbiased look at dataset bias. In *CVPR*. IEEE, 2011.

Florian Tramer, Fan Zhang, Ari Juels, Michael K Reiter, and Thomas Ristenpart. Stealing machine learning models via prediction APIs. In *25th USENIX security symposium (USENIX Security 16)*, pp. 601–618, 2016.

Minh-Tuan Tran, Trung Le, Xuan-May Le, Mehrtash Harandi, Quan Hung Tran, and Dinh Phung. Nayer: Noisy layer data generation for efficient and effective data-free knowledge distillation. In *CVPR*, 2024.

United States Congress. Health insurance portability and accountability act of 1996. Public Law 104-191, 110 Stat. 1936, 1996. URL `https://www.congress.gov/bill/104th-congress/house-bill/3103`. Enacted August 21, 1996.

United States Congress. Defend trade secrets act of 2016. Public Law 114–153, 130 Stat. 376, 2016. URL `https://www.congress.gov/bill/114th-congress/senate-bill/1890`. Enacted May 11, 2016.

Tri-Nhan Vo, Dang Nguyen, Kien Do, and Sunil Gupta. Improving diversity in black-box few-shot knowledge distillation. In *ECML-PKDD*. Springer, 2024.

Dongdong Wang, Yandong Li, Liqiang Wang, and Boqing Gong. Neural networks are more productive teachers than human raters: Active mixup for data-efficient knowledge distillation from a blackbox model. In *CVPR*, 2020.

Zhenyi Wang, Yihan Wu, and Heng Huang. Defense against model extraction attack by bayesian active watermarking. In *ICML*, 2024.

Zi Wang. Zero-shot knowledge distillation from a decision-based black-box model. In *ICML*, pp. 10675–10685. PMLR, 2021.

xAI. Grok 4 fast - pushing the frontier of cost-efficient intelligence, 2025. URL `https://x.ai/news/grok-4-fast`.

Han Xiao, Kashif Rasul, and Roland Vollgraf. Fashion-mnist: a novel image dataset for benchmarking machine learning algorithms. *arXiv:1708.07747*, 2017.

Junho Yim, Donggyu Joo, Jihoon Bae, and Junmo Kim. A gift from knowledge distillation: Fast optimization, network minimization and transfer learning. In *CVPR*, 2017.

Xiaojian Yuan, Kejiang Chen, Wen Huang, Jie Zhang, Weiming Zhang, and Nenghai Yu. Data-free hard-label robustness stealing attack. In *AAAI*, 2024.

Sangdoo Yun, Dongyoon Han, Seong Joon Oh, Sanghyuk Chun, Junsuk Choe, and Youngjoon Yoo. Cutmix: Regularization strategy to train strong classifiers with localizable features. In *ICCV*, 2019.

Jie Zhang, Chen Chen, and Lingjuan Lyu. Ideal: Query-efficient data-free learning from black-box models. In *ICLR*, 2022.

Appendix

In this extended text, we provide our implementation details (A), a complementary study on alternative optimization objectives for our image priors (B), and an extension to an iterative framework (C). Explicit results to the figures in the main text are also provided for completeness and reproducibility (D).

A Training Details

A.1 Datasets

In our experiments (Sec. 4), we evaluate our method on eight benchmark image datasets: MNIST (LeCun et al., 1998), USPS (Hull, 1994), SVHN (Netzer et al., 2011), FMNIST (Xiao et al., 2017), CIFAR10, CIFAR100 (Krizhevsky et al., 2009), TinyImageNet (Le & Yang, 2015), Imagenette (FastAI, 2020). All datasets are public and easily downloadable with standard libraries. In terms of image content, MNIST, USPS, and SVHN contain small images of digits. FMNIST is also a small-sized dataset of fashion items. The images in CIFAR10, CIFAR100, TinyImageNet, and Imagenette all contain diverse scenes and objects, e.g., animals, plants, food, vehicles, and household goods, to name a few. Notably, TinyImageNet and Imagenette have higher resolution: 64×64 for TinyImageNet, and approximately one magnitude larger than that for Imagenette (ranging from 27×80 to 4368×2912 — which we reported the average dimension). Of all the benchmarks, only CIFAR100 and TinyImageNet have abundant classes (100 and 200, respectively), while the others have 10 classes. Regarding the dataset size, USPS and Imagenette are relatively smaller. We summarize their details in Table A.1.

Table A.1: Details of the image benchmark datasets.

	Dataset	**Dimension**	**Size**		**No.**	**Content**
			train	test	**classes**	
Simple	MNIST	1×28×28	60 K	10 K	10	Digits
	USPS	1×16×16	9 K	2 K	10	Digits
	SVHN	3×32×32	73 K	26 K	10	Digits
	FMNIST	1×28×28	60 K	10 K	10	Fashion items
Complex	CIFAR10	3×32×32	50 K	10 K	10	Diverse
	CIFAR100	3×32×32	50 K	10 K	100	Diverse
	TinyImageNet	3×64×64	100 K	10 K	200	Diverse
	Imagenette	3×408×472▲	9 K	4 K	10	Diverse

▲: The average dimension of Imagenette is reported.

A.2 Teacher and students training

A.2.1 Augmentation

To augment the training data (real images for the teacher, synthetic images for students), we design a basic augmentation pipeline. Firstly, if the images are very small (in MNIST, USPS, FMNIST), we resize them to at least 32×32. Then the images undergo random shifting by 1/8 of their dimension, and random horizontal flipping unless they are from a digits dataset (MNIST, USPS, SVHN). Finally, we randomly jitter the color in the images for more image variety.

A.2.2 Optimization and scheduling

To train the Teacher for baseline, and the Students in our method, we use a stochastic gradient descent optimizer with momentum of 0.9, weight decay of 5×10^{-4}, and batch size of 100. On datasets with small black-and-white images (MNIST, USPS, FMNIST), we use a fixed learning rate of 10^{-2} and train for 100 epochs. On other datasets, we set the learning rate to 10^{-1} at the beginning and gradually decrease by two orders of magnitude with a scheduler to enable optimal convergence for 200 training epochs.

A.3 Optimization of Image Priors

A.3.1 Diverging filter

We provide more details on the formulation of the diverging filter f_{divg} (Eq. 5) proposed in the Synthesis phase (Sec. 3.1). To fulfill its role in contrasting opposite-type regions in a mask $m \in [0,1]^{C\times H\times W}$, we expect f_{divg} to satisfy the following properties:

1. We start by picking a brightness cutoff threshold β to separate the negative ($x < \beta$) and postive regions ($x \geq \beta$) for any pixel $x \in m$. The extrema and the threshold value must be fixed after filtering, i.e., $f_{\text{divg}}(\cdot;\beta)$ must go through $\{(0,0),(\beta,\beta),(1,1)\}, \forall\beta$.

2. To preserve the order of intensity across the whole mask, it is necessary that f_{divg} is an increasing function, i.e., $f'_{\text{divg}}(x;\beta) > 0, \forall x,\beta \in [0,1]$.

3. To avoid creating abrupt changes in intensity, i.e., f_{divg} must be continuously differentiable on $[0,1], \forall\beta$.

4. To ensure the diverging property emerges at the threshold value $x = \beta$, we require that f_{divg} has the sharpest increase there, i.e., $f'_{\text{divg}}(\cdot;\beta)$ has a maximum at $x = \beta \Leftrightarrow f''(x=\beta;\beta) = 0, f'(x=\beta;\beta) > 0$.

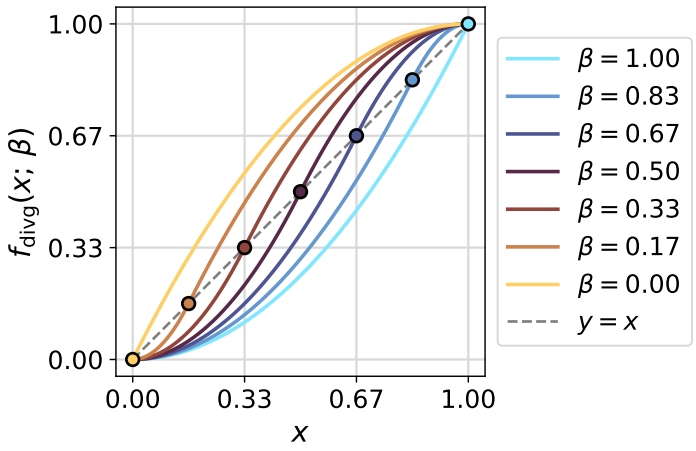

Figure A.1: Our diverging filter as $y = f_{\text{divg}}(x;\beta)\,|_{x\in[0,1]}$ in Eq. 5 with different choices of $\beta \in [0,1]$. Scattered points $\{(\beta,\beta)\}$ along the diagonal $y = x$ are also inflection points.

Accordingly, we design a piecewise function consisting of two continuously differentiable half-parabolas connected at the inflection point (β,β). One of them has a minimum at the $x = 0$ boundary, and vice versa, the other half-parabola has a maximum at the opposite boundary $x = 1$, i.e., $f'_{\text{divg}}(0;\beta) = f'_{\text{divg}}(1;\beta) = 0\forall\beta \in [0,1]$. Solving the two parabolas with the proposed set of constraints indeed gives the solution we reported f_{divg} in Eq. 5. We plot f_{divg} with a range of $\beta \in [0,1]$ values in Fig. A.1 to demonstrate its diverging property. We believe that this filter design has unexplored potentials in image augmentation for robust learning of vision tasks.

A.3.2 Loading unique embeddings during Contrast phase

In the Contrast phase, we apply the contrastive method proposed in Fang et al. (2021) to make our data diverse. However, we occasionally observed numerical inbstability and synthetic image corruption during contrastive optimization. After investigation, we found that the issue stems from how embeddings are loaded for contrastive learning. Originally, the embeddings of past inputs x and their corresponding positive views x^+ are cached to and recalled from an index-free memory bank. (The same occurred for negative samples,

but it is not linked to the error.) As a result, for small datasets, an embedding loaded from the memory bank might be near-duplicated with one extracted at runtime as, by chance, they may originate from the same image and differ by some trivial updates. Optimization-wise, contrasting an image against itself is counter-intuitive, which explains the exploding gradients and corruption of synthetic images.

Therefore, we modify how images are loaded for contrastive optimization. Instead of using an index-free memory bank, we store the embeddings of each synthetic images in our dataset by its unique index. At contrastive learning runtime, we only load embeddings of images **not** in the current batch, successfully avoid duplication. This modification fixes the numerical instability and synthetic image corruption on our ends.

A.3.3 Instance-discriminator

Following Fang et al. (2021), we use a fully connected instance-discriminator R comprising of two libear layers. For each input image x, R projects the image embedding $h = S_0^{\mathcal{H}}(x)$ from the primer student backbone $S_0^{\mathcal{H}}$, through one hidden layer, to its own embedding space of 128 dimensions. To update R during the Contrast phase (Sec. 3.2), we let the contrastive loss $\mathcal{L}_{\text{CT}}$ in Eq. 9 backpropagate to it parameters. It is trained with an Adam optimizer (Kingma & Ba, 2014) with a learning rate of 10^{-3}, and its "betas" coefficients of (0.5, 0.999). As R is shallow, this does not incur a significant computational overhead.

A.3.4 Resources

We perform each standard experiment on a single NVIDIA V100 GPU with 40GB VRAM, 4–16 CPUs, and 4–128 GB RAM, taking around 6–96 hours. The required resources depend on the dataset complexity, model size, and synthetic image resolution. In an increasing order, their training time rank as: simple datasets (negligible difference), CIFAR10, CIFAR100, Imagenette, and TinyImageNet.

B Alternative image optimization objectives

In the following section, we will examine student accuracy when adopting different optimization objectives for image prior optimization, and justify our choice of the contrastive approach for diversity. During the Contrast phase, we employ the contrastive loss $\mathcal{L}_{\text{CT}}$ in Eq. 9 to make synthetic images more diverse. Unlike the diversity objective in our framework, previous BBDFKD methods such as Zhang et al. (2022); Yuan et al. (2024) attempted to promote in-class similarity and class-balance. Specifically, in-class similarity is optimized via the one-hot loss:

$$\mathcal{L}_{\text{OH}} = \mathcal{L}_{\text{CE}}\left(\hat{y}_{S-\text{Soft}}, \text{argmax}(\hat{y}_{S-\text{Soft}})\right), \tag{B.1}$$

which guides data generation to strengthen the effect of the most prominent class in each sample. The one-hot loss is popular in data-free KD (Chen et al., 2019), but as stated in Yuan et al. (2024), its adversarial nature might cause "overfitting of synthetic data to the clone model", resulting in mode collapse and insufficient diversity.

The other objective, class-balance, is to ensure the samples are evenly distributed between all classes, enforced by the information entropy loss:

$$\mathcal{L}_{\text{IE}} = \sum_{k=0}^{K-1} p_k \log p_k, \text{ with } p_k = \mathbb{E}_{x\sim\mathcal{D}}\left[\hat{y}^{(k)}_{S-\text{Soft}}\right], \tag{B.2}$$

where k denotes the k-th class probability. In our framework, as we have actively balanced the dataset during sampling, class-balance has already been satisfied.

To measure how these objectives might affect KD performance, we ablate them using different losses to optimize the image priors dataset $\mathcal{D} = \{x | x \sim \mathcal{X}_{\mathcal{P}}\}$, on our standard MNIST and CIFAR10 experiments as the base cases. In details, we ran all eight binary combinations of using/not using $\mathcal{L}_{\text{OH}}$, $\mathcal{L}_{\text{IE}}$, $\mathcal{L}_{\text{CT}}$ to optimize $\mathcal{D}$, and report in Fig. B.1. The contribution of each objective is derived by the mean difference in student accuracy between using/not using the corresponding loss, while standard error is aggregated

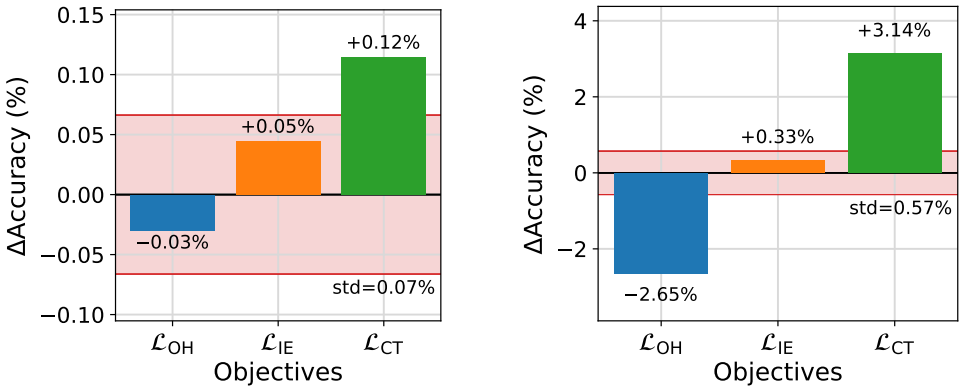

(a) MNIST **(b)** CIFAR10

Figure B.1: Contribution to distillation accuracy (%) of one-hot loss ($\mathcal{L}_{\text{OH}}$), information entropy loss ($\mathcal{L}_{\text{IE}}$), and contrastive loss ($\mathcal{L}_{\text{CT}}$), on MNIST and CIFAR10.

on a per-combination basis. We observe $\mathcal{L}_{\text{IE}}$ only has modest contribution, as class-balance has already been achieved during Synthesis. Surprisedly, in-class similarity $\mathcal{L}_{\text{OH}}$ is actually adversarially destructive, harming KD performance by a significant amount of -2.65%. Meanwhile, contrastive optimization using $\mathcal{L}_{\text{CT}}$ fruitfully helped gain KD performance, notably by $+0.12\%$ on MNIST and $+3.14\%$. Thus, we focus solely on diversity abd employ only the contrastive loss $\mathcal{L}_{\text{CT}}$ to optimize image priors.

On a side note, Zhang et al. (2022); Yuan et al. (2024) employed $\mathcal{L}_{\text{OH}}$ and $\mathcal{L}_{\text{IE}}$ on the weights of a generator network, while we employ $\mathcal{L}_{\text{CT}}$ on the parameterized image priors $\mathcal{X}_{\mathcal{P}}$ and an instance-discriminator R. We speculate that this difference also affects the comparision and requires further investigation.

C Extension to Iterative Framework

An interesting extension of our framework is performing *iterative Contrast-Distillation* to further boost student performance. Recall that in the Contrast phase (Sec. 3.2), we employ an primer student S_0 to optimize the dataset $\mathcal{D}$, and train a new student S in the next Distillation phase. It naturally emerges that the stronger S possesses even more robust embeddings and can be *recycled for Contrast phase again*. Iteratively, we may re-employ the latest student S_g at the g-th generation in the role of a new primer student to optimize $\mathcal{D}$ in the next Contrast phase, and query soft labels from it to train the new student S_{g+1} in the next Distillation phase. The objectives for S_{g+1}, extended from $\mathcal{L}_S$ (Eq. 10), is to match the teacher's label $T(x)$ with $\mathcal{L}_{\text{Hard-KD}}$, and to match previous student's logits $S_g^{\mathcal{Z}}(x)$ with $\mathcal{L}_{\text{Soft-KD}}$, on samples $x \sim \mathcal{D}$:

$$\mathcal{L}_{S_g} = \mathcal{L}_{\text{Hard-KD}} + \mathcal{L}_{\text{Soft-KD}} = \mathbb{E}_{x\sim\mathcal{D}}\Big[\mathcal{L}_{\text{CE}}\left(\hat{y}_{S_{g+1}-\text{Soft}}, \hat{y}_{T-\text{Hard}}\right) + \mathcal{L}_{\text{L1}}\left(S_{g+1}^{\mathcal{Z}}(x), S_g^{\mathcal{Z}}(x)\right)\Big]. \tag{C.1}$$

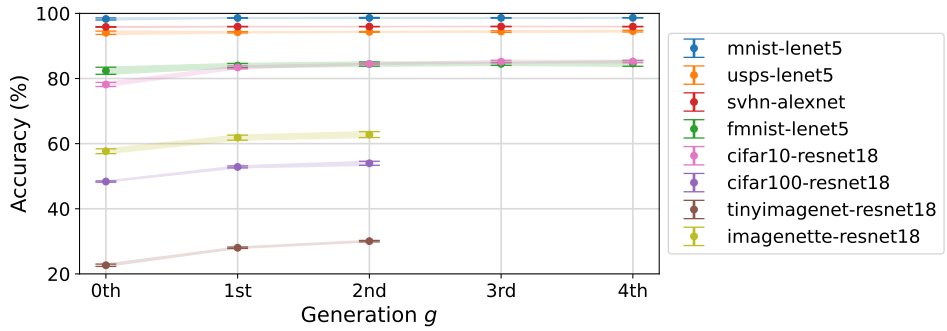

Figure C.1: Distillation accuracy (%) by generation g.

From our standard experiments (Sec. 4.3, corresponds to $g = 1$), we iterate for more generations to reach $g = 4$ on simple datasets and $g = 2$ on complex datasets due to resource constraints. As reported in Fig. C.1, even though KD performance converges quickly on simple dataset, it iteratively improves until the last generations with trivial fluctuations. These results conclude that our iterative Contrast-Distillation strategy can robustly deliver increasingly better students with more generations, and that generalization is not hurt with longer training. Nonetheless, computational cost increases *linearly* but student accuracy does not scale as fast to justify the trade-off. We look forward to making this extension even more efficient in future works.

D Explicit Results

In this section, we provide explicit numerical results for the figures presented in the main text and above sections of the Appendix for completeness and reproducibility.

D.1 Increasing synthetic dataset size

We provide explicit student accuracy and standard error for KD by number of samples, which has been visualized and discussed in Fig. 6, Sec. 4.4.4. The results are grouped by the simple datasets in Table D.1 and complex datasets in Table D.2.

Table D.1: Distillation accuracy (%) by number of sample N on simple datasets.

N	**MNIST** LeNet5	**USPS** LeNet5	**SVHN** AlexNet	**FMNIST** LeNet5
10 K	$98.20_{\pm.06}$	$93.22_{\pm.43}$	$94.64_{\pm.13}$	$76.14_{\pm2.48}$
20 K	$98.59_{\pm.08}$	$93.99_{\pm.24}$	$95.46_{\pm.07}$	$79.49_{\pm1.38}$
30 K	$98.68_{\pm.03}$	$94.05_{\pm.08}$	$95.71_{\pm.05}$	$82.67_{\pm .45}$
50 K	$98.75_{\pm.03}$	$94.20_{\pm.21}$	$95.94_{\pm.05}$	$83.98_{\pm .65}$
70 K	$98.81_{\pm.03}$	$94.25_{\pm.06}$	$95.97_{\pm.02}$	$84.84_{\pm .69}$
100 K	$98.78_{\pm.05}$	$94.41_{\pm.08}$	$96.06_{\pm.03}$	$\mathbf{85.63}_{\pm .39}$
128 K	$\mathbf{98.90}_{\pm.02}$	$\mathbf{94.44}_{\pm.09}$	$\mathbf{96.13}_{\pm.01}$	$85.62_{\pm .06}$

Best results are in **bold**.

Table D.2: Distillation accuracy (%) by number of samples N on complex datasets.

N	**CIFAR10**	**CIFAR100**	**TinyImageNet**	**Imagenette**
10 K	$63.54_{\pm2.64}$	$25.85_{\pm1.31}$	$07.88_{\pm.49}$	$50.82_{\pm1.65}$
20 K	$72.98_{\pm .50}$	$37.48_{\pm .48}$	$12.13_{\pm.17}$	$57.43_{\pm1.51}$
30 K	$78.18_{\pm .60}$	$42.82_{\pm .56}$	$13.96_{\pm.42}$	$58.98_{\pm1.19}$
50 K	$83.41_{\pm .46}$	$48.45_{\pm .26}$	$16.49_{\pm.37}$	$61.84_{\pm .77}$
70 K	$85.20_{\pm .35}$	$50.75_{\pm .18}$	$18.69_{\pm.63}$	$63.08_{\pm .96}$
100 K	$86.60_{\pm .29}$	$52.85_{\pm .30}$	$19.99_{\pm.36}$	$65.98_{\pm .78}$
128 K	$87.56_{\pm .11}$	$53.69_{\pm .26}$	$21.07_{\pm.50}$	$\mathbf{66.60}_{\pm .72}$
256 K	$\mathbf{89.24}_{\pm .15}$	$\mathbf{56.84}_{\pm .54}$	$24.46_{\pm.26}$	-
512 K	-	-	$\mathbf{28.06}_{\pm.22}$	-

Best results are in **bold**.

D.2 Students of compressed capacity

We provide in Table D.3 explicit student accuracy and standard error for KD by compression ratio, which has been visualized and discussed in Fig. 7, Sec. 4.4.7.

Table D.3: Distillation accuracy (%) by compression ratio (CR).

CR	**MNIST** LeNet5	**USPS** LeNet5	**SVHN** AlexNet	**FMNIST** LeNet5	**CIFAR10** ResNet18
100%	$98.59_{\pm .08}$	$94.20_{\pm .21}$	$95.94_{\pm .05}$	$83.98_{\pm .65}$	$83.41_{\pm .46}$
25%	$96.79_{\pm 1.39}$	$92.42_{\pm .08}$	$95.41_{\pm .04}$	$74.90_{\pm .37}$	$79.23_{\pm .51}$
4%	$85.83_{\pm 1.86}$	$90.70_{\pm .33}$	$92.51_{\pm .07}$	$52.55_{\pm 3.79}$	$64.48_{\pm .81}$
1%	$47.72_{\pm 7.44}$	$52.43_{\pm 1.47}$	$72.00_{\pm 2.89}$	$36.85_{\pm 8.66}$	$47.39_{\pm 3.30}$

D.3 Extension to Iterative Framework

We provide explicit student accuracy and standard error for KD by number of generations, which has been visualized and discussed in Fig. C.1, Sec. D.3. We ran the experiments for all datasets, but limits to $g = 2$ on complex dataset due to resource constraints, as shown in Table D.4. We additionally remark that the student can get iteratively better until the last generations, with some trivial fluctuations.

Table D.4: Distillation accuracy (%) by generation g.

g	MNIST LeNet5	USPS LeNet5	SVHN AlexNet	FMNIST LeNet5	CIFAR10 ResNet18	CIFAR100 ResNet18	Tiny$^{(*)}$ ResNet18	Nette$^{(**)}$ ResNet18
0	$98.29_{\pm .32}$	$94.04_{\pm .52}$	$95.84_{\pm .10}$	$82.38_{\pm 1.09}$	$78.17_{\pm .64}$	$48.36_{\pm .19}$	$22.66_{\pm .36}$	$57.67_{\pm .74}$
1	$98.59_{\pm .08}$	$94.20_{\pm .21}$	$95.94_{\pm .05}$	$83.98_{\pm .65}$	$83.41_{\pm .46}$	$52.85_{\pm .30}$	$28.03_{\pm .22}$	$61.84_{\pm .77}$
2	$98.62_{\pm .12}$	$94.32_{\pm .12}$	$95.95_{\pm .03}$	$84.43_{\pm .66}$	$84.50_{\pm .16}$	$\mathbf{53.97}_{\pm .62}$	$\mathbf{30.06}_{\pm .22}$	$\mathbf{62.78}_{\pm .91}$
3	$98.61_{\pm .08}$	$94.42_{\pm .25}$	$\mathbf{95.97}_{\pm .06}$	$84.50_{\pm .46}$	$85.18_{\pm .42}$	-	-	-
4	$\mathbf{98.65}_{\pm .04}$	$\mathbf{94.54}_{\pm .25}$	$95.94_{\pm .06}$	$\mathbf{84.62}_{\pm .86}$	$\mathbf{85.23}_{\pm .39}$	-	-	-

Best results are in **bold**. $^{(*)}$TinyImageNet, $^{(**)}$Imagenette